

A case study of comparing two dimerized acceptor molecules built by different branch-connected and terminal-connected approaches

Kangqiao Ma^{1†}, Huazhe Liang^{1†}, Yuxin Wang¹, Tengfei He², Tainan Duan³, Xiaodong Si¹, Wendi Shi¹, Guankui Long², Xiangjian Cao¹, Zhaoyang Yao^{1*}, Xiangjian Wan¹, Chenxi Li¹, Bin Kan² & Yongsheng Chen^{1*}

¹State Key Laboratory and Institute of Elemento-Organic Chemistry, Frontiers Science Center for New Organic Matter, The Centre of Nanoscale Science and Technology and Key Laboratory of Functional Polymer Materials, Institute of Polymer Chemistry, Renewable Energy Conversion and Storage Center (RECAST), College of Chemistry, Nankai University, Tianjin 300071, China;

²School of Materials Science and Engineering, National Institute for Advanced Materials, Renewable Energy Conversion and Storage Center (RECAST), Nankai University, Tianjin 300350, China;

³Chongqing Institute of Green and Intelligent Technology, Chongqing School, University of Chinese Academy of Sciences (UCAS Chongqing), Chinese Academy of Sciences, Chongqing 400015, China

Received November 8, 2023; accepted January 5, 2024; published online March 29, 2024

Dimerized small-molecule acceptors (SMAs) built by the conventional connection of terminal groups of monomers have contributed to exciting long-term stabilities of organic solar cells (OSCs). However, device efficiencies, especially fill factors (FFs), still need to be improved. This probably originates from unsymmetrical molecular structure/conformation-determined less compact/ordered molecular stackings, such as ineffective stackings of constraint terminals. Herein, an exotic dimerized SMA of BC-Th is established by bridging the branched groups (BC-type, branch coupling) of two monomers rather than conventional terminal units (TC-type, terminal coupling). Benefiting from the three-dimensional conformation and more uncurbed terminals, BC-Th exhibits multiple molecular orientations along with a larger dielectric constant and electron mobility compared with TC-Th. Finally, an efficiency of 17.43% is achieved by BC-Th-based OSCs, along with the highest FF of 79.13% among all dimerized SMAs-based OSCs to date. When introducing L8-BO as the third component, overall enhanced efficiency of 18.05% and FF of 80.11% are further afforded. Contrarily, TC-Th-based OSCs exhibit much inferior PCE of 16.29% and FF of 74.81%, demonstrating the great advantages of “branch coupling” over “terminal coupling” when building dimerized SMAs.

organic solar cells, dimerized acceptor molecules, branch coupling, morphology control, stability

Citation: Ma K, Liang H, Wang Y, He T, Duan T, Si X, Shi W, Long G, Cao X, Yao Z, Wan X, Li C, Kan B, Chen Y. A case study of comparing two dimerized acceptor molecules built by different branch-connected and terminal-connected approaches. *Sci China Chem*, 2024, 67, <https://doi.org/10.1007/s11426-023-1923-4>

1 Introduction

Organic solar cells (OSC) have been regarded as the next-generation photovoltaic technology due to their high light acquisition ability, excellent flexibility, low cost, and tunable

transparency [1–4]. Recent years have witnessed the significant development of small-molecule acceptors (SMAs) that feature an acceptor-donor-acceptor (A-D-A) structure, boosting power conversion efficiencies (PCEs) over 19% in single junction- and over 20% in tandem-OSCs [5–11]. Since the PCEs of OSCs have achieved the stage that is likely to meet the requirements for commercial viability, more and more efforts have been devoted to conquering the challenges

[†]These authors contributed equally to this work.

*Corresponding authors (email: zyao@nankai.edu.cn; yschen99@nankai.edu.cn)

of unsatisfied long-term operational stability [12–14]. Note that one of the most crucial reasons for device degradation should be the diffusion of small-molecule acceptors (SMAs) in blended films during the evolution from a dynamic equilibrium state to a thermodynamic one [15–17]. Thus, enlarging the molecular size of acceptors to decrease molecular diffusion coefficients, such as developing SMAs of dimers, trimers, and polymers, is becoming an effective strategy to improve device stability and, at the same time, maintain a decent efficiency [18–21].

Presently, nearly all high-performance giant molecular acceptors, including dimers, trimers, and polymers, are constructed by directly coupling electron-deficient terminals (TC-type) of Y-series SMAs [22–25]. However, this constructing pathway would result in several inherent disadvantages. (1) Insufficient intermolecular packing. By analyzing lots of single-crystal structures for well-known Y-series SMAs, it can be revealed that the effective molecular packings through both terminal and central units are crucially important for constructing desirable three-dimensional (3D) packing networks [26–28]. Nevertheless, the chemical structure, electronic characteristics, and spatial environments of terminal units will be significantly impacted if coupling happens at the end unit with various linker units (like thiophene and its analogs) [15,29–32]. In this way, the nearing perfect molecular packing already formed by Y-series SMAs will be hindered inevitably, thus harming the performance of resulting OSCs. (2) Reduced halogen density on molecular backbones. The pathway to construct dimerized SMAs through terminal coupling will occupy two halogenated active sites [33–35]. However, the halogens on terminals have been proven to effectively induce more favorable molecular packing of SMAs and also more efficient charge migration dynamics in OSCs. (3) Spatial isomerization. Currently, the widely employed terminal units are 1,1-dicyanomethylene-3-indanone (IC) and its halides [36]. Pre-brominating on IC is usually essential to carrying out the terminal coupling successfully. Unfortunately, a mixture of two brominated isomers will be afforded due to the lack of selectivity. Meanwhile, it is very difficult to purify in light of their highly similar polarity [37,38]. If the problem of spatial isomerization remains in target SMAs, the PCEs of resulting OSCs will usually be decreased [39]. In spite of the exciting long-term stabilities, all the deficiencies mentioned above render that the PCE for giant molecular acceptor-based OSCs may not be as high as their monomer counterparts ultimately, especially for FFs that are closely associated with molecular stacking strength/modes. Therefore, establishing more compact/ordered molecular stackings for giant molecular acceptors through some innovative pathways to delicately optimize molecular structure/conformation should be crucially important for OSCs that feature both long-term stabilities and excellent PCEs.

Bearing these thoughts in mind, an exotic pathway to construct dimerized SMAs was explored by bridging branched groups of two monomers to obtain BC-Th acceptor (BC-type, branch coupling). Its counterpart of TC-Th (TC-type, terminal coupling) was also synthesized through conventional terminal units, as shown in Figure 1a. Note that BC-Th and TC-Th have almost identical molecular compositions but possess only one major difference in molecular coupling sites. Benefiting from the three-dimensional conformation and less disturbed terminals, the BC-type acceptor of BC-Th exhibits multiple molecular orientations along with a larger molar extinction coefficient, dielectric constant, and electron mobility compared with the TC-type acceptor of TC-Th. Moreover, BC-Th-based blended films have better compact/ordered molecular stacking and clear fibrillary networks to afford facilitated charge migration and suppressed recombination. Thus, the binary device of BC-Th:D18 achieves a PCE of 17.43%, along with an excellent FF of 79.13%. Notably, the FF should be the highest value among dimerized SMAs-based OSCs (Table S1, Supporting Information online). On the contrary, a similar device based on TC-Th exhibits only the PCE of 16.29% and the FF of 74.81%. Furthermore, the ternary device of BC-Th, with L8-BO as the third component, could achieve a remarkable FF of 80.11% and a better efficiency of 18.05%. Also, BC-Th:D18-based devices show much improved device stability ($T_{80} = 372$ h) compared with TC-Th:D18-based ones ($T_{80} = 244$ h). These results demonstrate that by exploring such an exotic constructing strategy of dimerized SMAs, a potential pathway to achieve highly stable OSCs without sacrificing too much device efficiencies.

2 Results and discussions

The chemical structures of the Y-Th monomer, BC-Th, and TC-Th dimers were exhibited in Figure 1a, and detailed synthesis procedures were presented in Scheme S1 (Supporting Information online). The nuclear magnetic resonance (NMR) spectra and matrix-assisted laser desorption/ionization time-of-flight (MALDI-ToF) mass spectrometry were presented in Figures S12–S25 (Supporting Information online). All the molecules have a good solubility in common solvents for device fabrication, such as chloroform (BC-Th, 40 mg/mL; TC-Th, 55 mg/mL) and chlorobenzene.

For current mainstream TC-type dimerized acceptors that couple through electron-deficient terminals, the red shift of maximum absorption peaks ($\Delta\lambda$) from solution to thin film is about 60 nm, significantly smaller than that of corresponding monomers (76–90 nm, detailed data is summarized in Table S1 for dimer systems with current efficiency of over 17%), suggesting the decreasing strength of molecular stacking for dimerized SMAs. Given that the weaker intermolecular in-

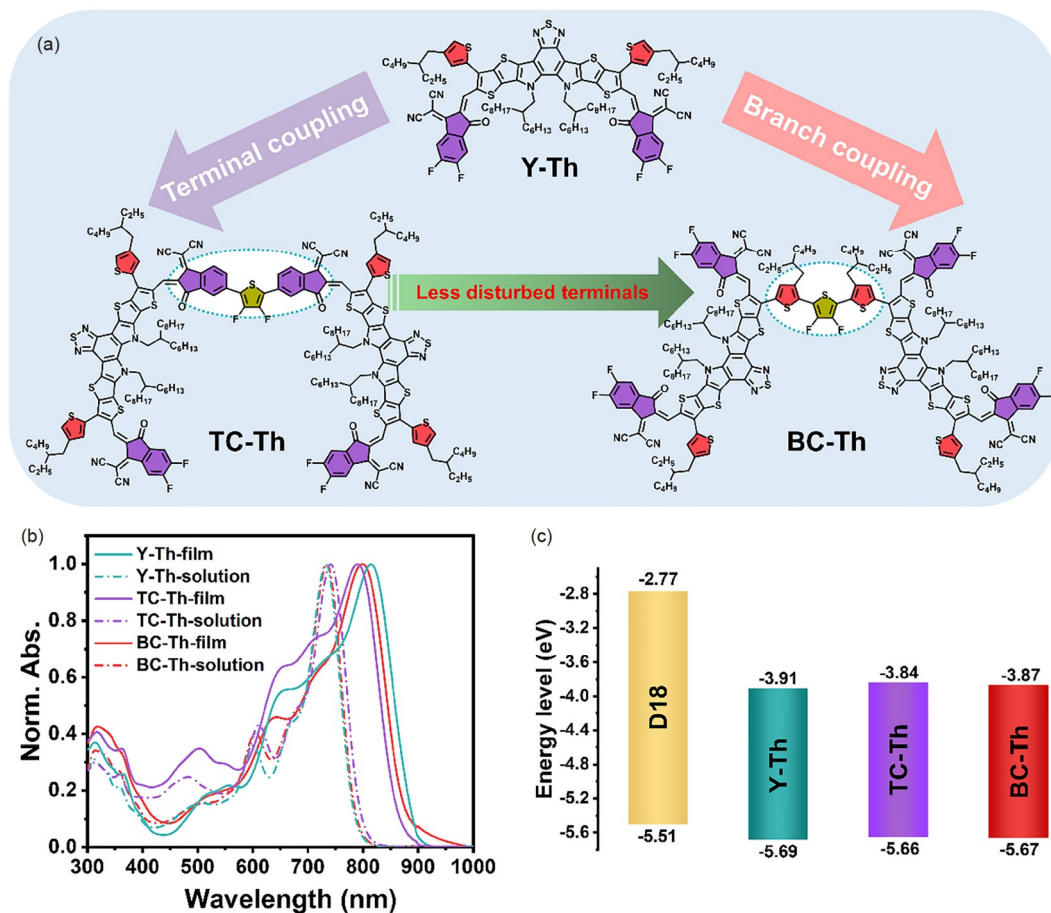


Figure 1 (a) Molecular structures of Y-Th, TC-Th and BC-Th. (b) Absorption spectra of Y-Th, TC-Th, and BC-Th in chloroform solutions and solid films. (c) Energy level alignments derived from CV (color online).

interactions usually lead to localized excitons with small exciton radius and large binding energies [40], carrier transport (electrons, holes) is also hindered because of the large energy barrier for hopping [41]. This could also be the main reason for the unsatisfactory device efficiencies, especially for FFs, compared with monomers at present. As discussed above, the exotic BC-type dimerized SMA of BC-Th in this study, established by bridging branched groups of two monomers rather than conventional terminal units, were expected to leave less disturbed terminals and further enhance intermolecular stacking. Therefore, it is plausible to observe an enlarged $\Delta\lambda$ of 65 nm for BC-Th from solution to thin film with respect to that of 49 nm for TC-Th (Figure 1b and Table 1). The molar extinction coefficients at maximum absorption (ϵ_{\max}) were estimated to be 2.06×10^5 and 2.22×10^5 L mol⁻¹ cm⁻¹ for TC-Th and BC-Th, respectively (Table 1 and Figure S1, Supporting Information online). Moreover, the onset absorption (λ_{onset}) of TC-Th and BC-Th films are 877 and 885 nm, respectively (Table 1). The larger ϵ_{\max} and red-shifted λ_{onset} for BC-Th indicate more powerful light harvesting ability, especially for low-energy photons, which could be in favor of a higher J_{SC} in resulting OSCs [42,43]. In

addition, the extended conjugated backbones of TC-Th and BC-Th are larger than those of monomers, which should be the main reason for the red shift of their absorption spectra in solutions. Cyclic voltammetry (CV) was further performed in order to unveil alignments of the highest occupied molecular orbitals (HOMOs) and lowest unoccupied molecular orbitals (LUMOs) of two dimers (Figure S2). The HOMO/LUMO energy levels for TC-Th and BC-Th derived from CV measurements are $-5.66/-3.84$ and $-5.67/-3.87$ eV, respectively (Figure 1c and Table 1). The similar HOMO and slightly down-shifted LUMO for BC-Th compared with TC-Th contribute to a smaller bandgap, which is in good agreement with the red-shifted absorption of BC-Th. To clarify the variation from monomer to two different types of dimers, BC-type BC-Th and TC-type TC-Th, we also listed the fundamental physicochemical data of Y-Th in Table 1. Apparently, both TC-Th and BC-Th demonstrate the blue-shifted absorption compared with that of Y-Th. However, BC-Th possesses the maximum absorption peak in films close to the Y-Th film, suggesting their more similar stacking behaviors and thus, possibly excellent FFs for OSCs based on both BC-Th and Y-Th. Compared with the Y-Th mono-

Table 1 The optical and electrochemical properties of Y-Th, TC-Th, and BC-Th

Molecule	$\lambda_{\max}^{\text{solution}}$ (nm)	$\lambda_{\max}^{\text{film}}$ (nm)	$\Delta\lambda$ (nm)	λ_{onset} (nm)	$E_{\text{g}}^{\text{opt a)}$ (eV)	HOMO (eV)	LUMO (eV)	$E_{\text{g}}^{\text{CV b)}$ (eV)	$\epsilon_{\text{max}}^{\text{c)}$ $(\text{M}^{-1} \text{cm}^{-1})$
Y-Th	732	815	83	898	1.38	-5.69	-3.91	1.78	1.89
TC-Th	741	790	49	877	1.41	-5.66	-3.84	1.82	2.06
BC-Th	734	799	65	885	1.40	-5.67	-3.87	1.80	2.22

a) $E_{\text{g}}^{\text{opt}}$ is estimated by the equation $E_{\text{g}} = 1240/\lambda_{\text{onset}}$; b) E_{g}^{CV} is estimated by the difference between HOMO and LUMO energy levels. c) The molar extinction coefficients in chloroform solution for TC-Th and BC-Th with $3 \times 10^{-6} \text{ mol L}^{-1}$.

mer, the up-shifted LUMO energy levels can be observed for both TC-Th and BC-Th, which is conducive to obtaining a larger open circuit voltage in theory. Due to the high novelty of constructing dimer molecules through branch coupling rather than terminal coupling, the following investigation will focus on the comprehensive comparison of TC-Th and BC-Th.

Density functional theory (DFT) was further applied to disclose the variation of molecular geometries caused by two different coupling strategies during the construction of dimerized SMAs. As shown in Figure 2a, TC-Th and BC-Th exhibit significant conformational differences. Among them, the former possesses an S-shape conformation and a relatively small dihedral angle between two conjugated monomer planes. The latter adopts a C-shape back-to-back symmetrical conformation along with a large dihedral angle between two monomer-conjugated planes, making the linear molecular skeleton multi-dimensional (Figure S3). Generally, the unique multi-dimensional structure of BC-Th with conjugation extension in multiple directions is expected to result in much different molecular stacking behaviors and morphological features in blended films [44]. Therefore, grazing incidence wide-angle X-ray scattering (GIWAXS) measurements were further carried out to disclose the molecular stacking orientations of dimerized SMAs. As illustrated in Figure 2b, c, TC-Th neat film exhibits the apparent π - π stacking (010) diffraction peaks, which are mainly located in the out-of-plane (OOP) direction. Moreover, the lamellar stacking (100) diffraction peaks mainly appear in in-plane (IP) directions, indicative of a prior face-on orientation in TC-Th neat films. In sharp contrast, BC-Th exhibits strong π - π stacking (010) and lamellar stacking (100) diffraction peaks in both IP and OOP directions, indicating that edge-on and face-on orientations coexist in BC-Th neat films [45,46]. However, TC-Th showed a smaller π - π stacking distance of 3.97 Å than that of 4.10 Å for BC-Th in the OOP direction (Table S2, Supporting Information online), BC-Th in turn possesses a tighter π - π stacking with a distance of 4.27 Å comparing with that of 4.52 Å for TC-Th in IP direction. This should be induced by the 3D molecular conformation of BC-Th, which may also contribute to an enlarged molecular packing density and, hence, improved relative dielectric

constants [44,47]. In addition, a similar crystal coherence length (CCL) of ~ 16.7 Å in the OOP direction for both TC-Th and BC-Th. However, an obviously enlarged CCL of 13.6 Å for BC-Th compared with that of 10.2 Å for TC-Th in the IP direction (Table S2) can be observed, suggesting the more ordered molecular packings for BC-Th in general. In order to verify the dielectric properties of two dimerized SMAs, the relative dielectric constant (ϵ_r) was further measured (Figure S4). It is worth noting that BC-Th shows a

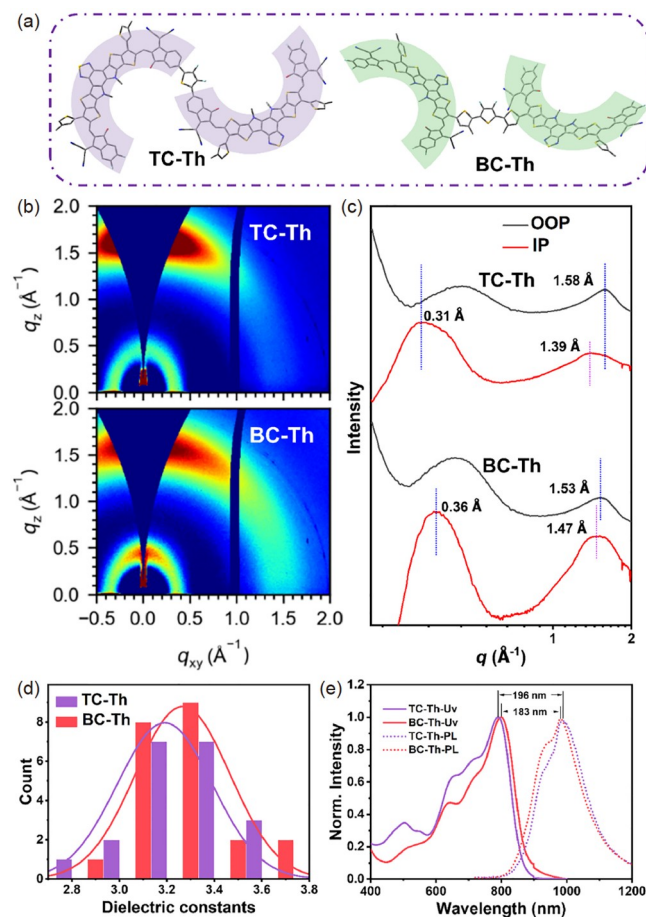


Figure 2 (a) Optimized molecular geometries of TC-Th and BC-Th. (b) 2D GIWAXS patterns of TC-Th and BC-Th pristine films. (c) 1D GIWAXS profiles of TC-Th and BC-Th pristine films. (d) Statistical distribution of dielectric constant results for TC-Th and BC-Th pristine film using over 20 devices. (e) Normalized absorption and PL spectra of TC-Th and BC-Th films (color online).

larger average ϵ_r of 3.3 (statistical results from more than twenty devices) than that of 3.1 for TC-Th in their neat films (Figure 2d). The enlarged ϵ_r could lead to an improved charge migration dynamic in theory and thus endow with BC-Th-based OSCs a better FF and J_{SC} [48,49]. Moreover, the electron mobilities of TC-Th and BC-Th neat films have been evaluated through the space charge limited current (SCLC) method [50]. As illustrated in Figure S5a, b, BC-Th displays a higher average electron mobility ($\mu_e = 2.4 \times 10^{-4} \text{ cm}^{-2} \text{ V}^{-1} \text{ s}^{-1}$) than that of TC-Th ($\mu_e = 2.0 \times 10^{-4} \text{ cm}^{-2} \text{ V}^{-1} \text{ s}^{-1}$). As we know, the charge mobility of organic semiconductors is tightly associated with molecular reorganization energies based on nonadiabatic semiclassical Marcus charge-transfer theory [51]. Therefore, the reorganization energies of TC-Th and BC-Th were roughly estimated by measuring their Stokes Shifts ($\Delta\lambda$, defined as the gap between the maximum absorption and photoluminescence peaks) [52,53]. As displayed in Figure 2e, the BC-Th film shows a relatively smaller $\Delta\lambda$ value of 183 nm than that of 196 nm for TC-Th, indicating the reduced reorganization energies from TC-Th to BC-Th and also is consistent with electron mobility results [54].

The quite different construction strategies for dimerized SMAs discussed above have given rise to remarkable variations of physicochemical properties and molecular packing behaviors, which should also exert significant influences on the photovoltaic performance of OSCs based on these two different types of dimers. Therefore, OSCs with conventional structure (Figure 3a) were fabricated by choosing D18 polymer as an electron donor to blend with BC-Th and TC-Th because of its well-matched energy levels and complementary absorptions [55]. The device fabrication condi-

tions have been carefully screened and the detailed device parameters are listed in Tables S3–S5. Among them, the best J - V characters for TC-Th- and BC-Th-based OSCs were presented in Figure 3b and the best photovoltaic data were enumerated in Table 2. OSCs based on BC-Th:D18 blend exhibit a remarkable PCE of 17.43% with a V_{OC} of 0.893 V, J_{SC} of 24.67 mA cm^{-2} and FF of 79.13%, which is generally better than TC-Th:D18-based devices (modest PCE of 16.29% with V_{OC} of 0.909 V, J_{SC} of 23.96 mA cm^{-2} and FF of 74.81%). Compared with TC-Th-based devices, the V_{OC} of BC-Th-based ones decreases slightly, which should be ascribed to the down-shifted LUMO energy levels of BC-Th compared with TC-Th [56,57]. On the other hand, the FF and J_{SC} of BC-Th-based OSCs are obviously higher than that of TC-Th-based ones, which can be ascribed to facilitated charge migration in BC-Th blended films (discussed below in detail). To our knowledge, the obtained FF of 79.13% for BC-Th-based OSCs is the highest value for dimers-based OSCs, including binary and ternary devices to date (Figure 3c and Table S1). This manifests great effectiveness in improving the FFs of OSCs by constructing dimerized SMAs through bridging branched groups of two monomers rather than conventional electron-withdrawing terminals. To further exploit the potential of dimerized BC-Th in photoelectric devices, L8-BO was added as the third component into BC-Th:D18 blends to construct a ternary device. As shown in Table 2, when employing L8-BO as a third component, both J_{SC} (25.55 mA cm^{-2}) and FF (80.11%) of ternary OSCs improved simultaneously, rendering an excellent PCE of 18.05%. From the external quantum efficiency (EQE) spectra (Figure 3d), it can be seen that both BC-Th-based OSCs exhibit stronger photo-response than

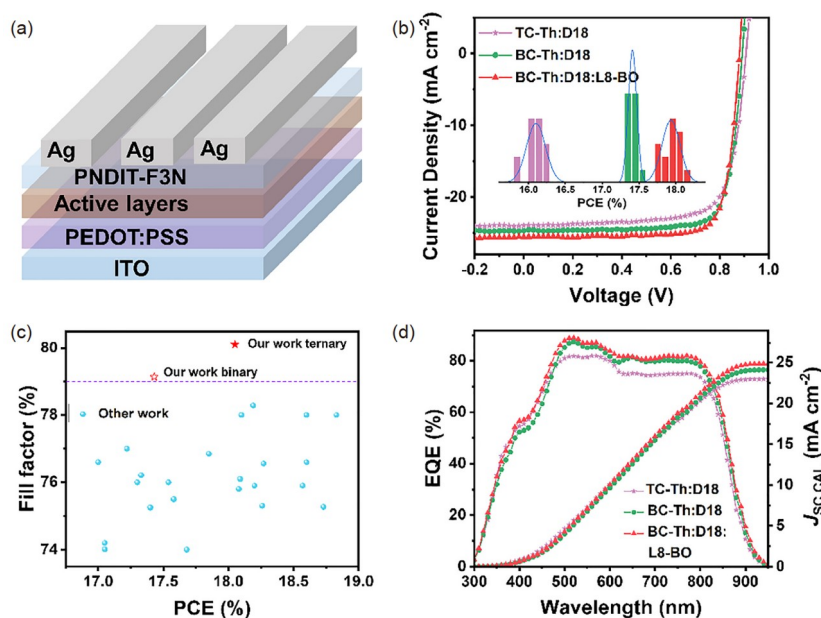


Figure 3 (a) Device structure of OSCs. (b) J - V characteristics of OSCs. (c) FF alignments of all dimer acceptor-based OSCs with PCE over 17%. (d) The EQE spectra of OSCs (color online).

TC-Th-based ones from 400 to 850 nm. The J_{SC} values integrated from EQE spectra are 22.95, 24.09 and 24.88 mA cm^{-2} for OSCs based on TC-Th:D18, BC-Th:D18 and BC-Th:D18:L8-BO-based devices, respectively, in accordance with the J_{SC} values derived from their J - V curves. The facilitated charge migration dynamics could account for the vastly improved J_{SC} and EQEs for TC-Th:D18, BC-Th:D18, and BC-Th:D18:L8-BO-based OSCs and the inner mechanism for photovoltaic performance upgrade will be further uncovered below. In addition, OSCs based on Y-Th:D18 achieved a PCE of 17.68% with a V_{OC} of 0.862 V, J_{SC} of 26.09 mA cm^{-2} , and FF of 78.62% (Figure S6a, b). The comparable and even better device efficiencies and FFs for BC-Th-based OSCs compared with its monomer of Y-Th manifest the advantages of constructing dimerized SMAs through branch coupling rather than terminal coupling. Therefore, accompanied by considerably better device stability (discussed below), the great possibility of commercial

applications has been fully unveiled for dimerized SMAs constructed by branch coupling.

Multiple photodynamic measurements were carried out to clarify the photovoltaic parameter difference of OSCs induced by two constructing strategies of dimerized SMAs. Firstly, we resorted to SCLC to evaluate the hole (μ_h)/electron mobilities (μ_e) of TC-Th:D18, BC-Th:D18 and BC-Th:D18:L8-BO-based devices (Figure 4a), being $1.11 \times 10^{-4}/1.40 \times 10^{-4}$, $1.29 \times 10^{-4}/1.55 \times 10^{-4}$ and $1.35 \times 10^{-4}/1.61 \times 10^{-4} \text{ cm}^2 \text{ V}^{-1} \text{ s}^{-1}$, respectively (Figure S7 and Table S6) [50,58]. Despite the gradually increased μ_h and μ_e from TC-Th:D18, BC-Th:D18 and BC-Th:D18:L8-BO blends, more balanced charge carrier mobility ($\mu_h/\mu_e = 0.83$ for BC-Th:D18, 0.84 for BC-Th:L8-BO:D18) than that of TC-Th:D18 ($\mu_h/\mu_e = 0.79$) can also be observed. All factors above work together to improve the J_{SC} and FF for BC-Th:D18 and BC-Th:D18:L8-BO-based devices, thus further leading to enhanced photovoltaic performances. Then, the photo-

Table 2 Optimized device performance of OSCs under the illumination of AM 1.5 G, 100 mW cm^{-2} a)

Active layers	V_{OC} (V)	J_{SC} (mA cm^{-2})	J_{SC}^{cal} (mA cm^{-2}) ^{b)}	FF (%)	PCE (%)
TC-Th:D18	0.909 (0.907 ± 0.002)	23.96 (23.80 ± 0.11)	22.95	74.81 (74.54 ± 0.53)	16.29 (16.10 ± 0.12)
BC-Th:D18	0.893 (0.889 ± 0.005)	24.67 (24.81 ± 0.13)	24.09	79.13 (79.00 ± 0.44)	17.43 (17.41 ± 0.06)
BC-Th:D18:L8-BO	0.882 (0.881 ± 0.003)	25.55 (25.65 ± 0.18)	24.88	80.11 (79.36 ± 0.53)	18.05 (17.94 ± 0.12)

a) The average photovoltaic parameters were calculated from 15 independent devices; b) current densities were calculated from EQE plots.

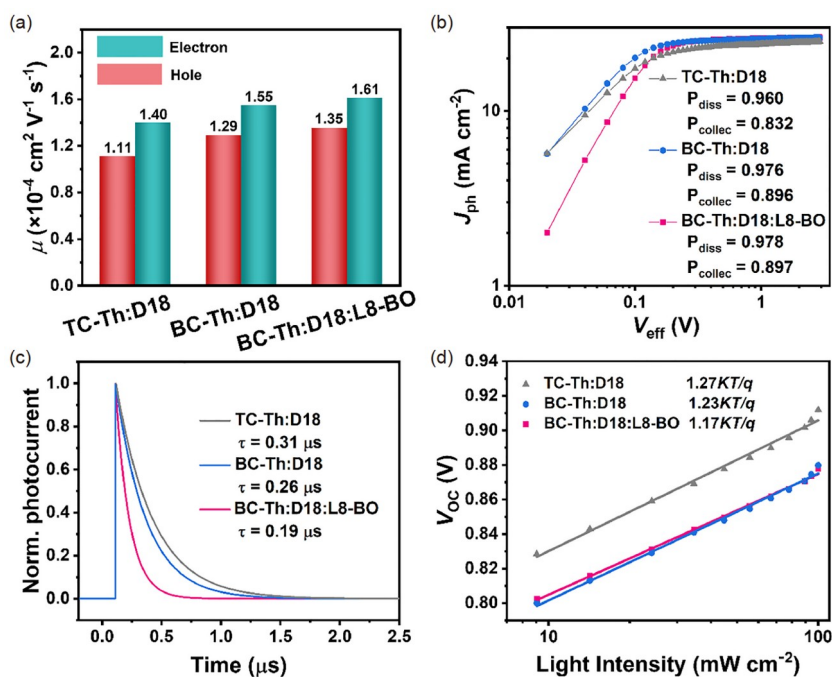


Figure 4 (a) Hole and electron mobilities of TC-Th:D18, BC-Th:D18, and BC-Th:D18:L8-BO based devices. (b) Plots of J_{ph} versus V_{eff} . (c) Transient photovoltage measurement for optimized OSCs. (d) Dependences of V_{OC} on P_{light} of optimized OSCs (color online).

generated current density (J_{ph}) against effective voltage (V_{eff}) measurement was conducted to unveil charge generation/collection processes in OSCs (Figure 4b) [59]. All the OSCs show the exciton dissociation probability (P_{diss}) approaching unit, whereas slightly larger for BC-Th:D18 (0.976) and BC-Th:D18:L8-BO (0.978) based devices compared with that of TC-Th:D18-based one (0.960). As regards the charge collection probability (P_{coll}), BC-Th:D18 and BC-Th:D18:L8-BO-based devices were estimated to be 0.896 and 0.897, also slightly higher than TC-Th-based optimal devices (0.832). These results indicate that more efficient charge generation and collection processes occurred in BC-Th-based OSCs, which are consistent with their enlarged J_{SC} compared with TC-Th-based ones. To further shed light on charge recombination and extraction behaviors in OSCs, transient photocurrent (TPC) and transient photovoltage (TPV) were investigated. As shown in Figure 4c, BC-Th:D18-based device shows a slightly faster extraction time of 0.26 μs than the device based on TC-Th:D18 (0.31 μs). Moreover, the ternary device affords the shortest charge extraction time of 0.19 μs . The stepwise faster charge extractions are in good agreement with their gradually increased charge mobility and $\mu_{\text{h}}/\mu_{\text{e}}$ ratios. The charge carrier lifetimes (τ) derived from TPV measurements are 0.13 ms for TC-Th:D18-, 0.18 ms for BC-Th:D18- and 0.21 ms for BC-Th:D18:L8-BO-based devices (Figure S8a), suggesting suppressed charge recombination in BC-Th-based binary and ternary devices [60,61]. Finally, the P_{light} dependence of J_{SC} , which can be described as $J_{\text{SC}} \propto P_{\text{light}}^S$, was analyzed to disclose the charge recombination mechanism. The power law exponent S usually indicates the degree of bimolecular charge recombination in OSCs [62]. All the devices exhibit equal and close unit S values of 0.99, indicating weaker and negligible bimolecular recombination (Figure S8b). According to plots showing the P_{light} dependence of V_{OC} (Figure 4d), the slope value can be regarded as an indicator of the degree of trap-state assisted charge recombination under open-circuit conditions [63]. TC-Th:D18-, BC-Th:D18- and BC-Th:D18:L8-BO-based devices afforded slopes of 1.27, 1.23 and 1.17 kT/q , respectively. The slope for BC-Th-based devices, which is closer to a unit, is indicative of suppressed Shockley-Read-Hall recombination [64,65].

Transmission electron microscopy (TEM) and tapping-mode atomic force microscopy (AFM) were applied to unveil the bulk and surface morphologies of blended films, respectively. The TEM pattern of the TC-Th:D18 blend exhibits featureless and homogenous textures. However, the stronger aggregated clusters emerged in both BC-Th:D18 and BC-Th:D18:L8-BO blends, suggesting better domain connectivity (Figure 5a). As shown in Figure S9, due to the strong aggregation property of D18 [66], all the blends offer similar and typical fibril networks with significant phase separation. The root mean square (RMS) roughness value of

BC-Th:D18:L8-BO (0.84 nm) is slightly smaller than that of BC-Th:D18 (1.00 nm) and TC-Th:D18 (0.92 nm) (Figure 5b), which may be one of the reasons for its more efficient charge generation/extraction processes. According to the GIWAXS discussions above, the neat film of TC-Th possesses the desirable face-on prior orientation, but BC-Th shows coexisted edge-on and face-on orientations. After blending with the D18 donor, the (010) diffraction peaks in TC-Th and BC-Th-based blends only appeared in the OOP direction and the (100) diffraction peaks only emerged in the IP direction, indicating the preferred face-on arrangements for all the blends (Figure 5c) [67]. This face-on arrangement is beneficial for the charge migration from the interfaces of the D/A domain towards electrodes [68]. Furthermore, as shown in Figure 5d and Table S7, BC-Th:D18 blend possesses a slightly smaller π - π distance of 3.83 \AA than that of 3.88 \AA for TC-Th:D18 blends, and the π - π stacking CCL for BC-Th:D18 blends is also larger than TC-Th:D18 blends. In addition, after adding L8-BO as the third component to BC-Th:D18 blends, the ternary blended film gives rise to a tighter π - π stacking and larger CCL than binary one, suggesting more compact and ordered molecular packing for BC-Th:L8-BO:D18 blends. This should be a response to the improved charge transfer/transport dynamics and also photovoltaic parameters for ternary devices.

Then, we further disclose the phase separation in blended films by evaluating D/A miscibility derived from the contact angle measurements (Figure S10). Note that the miscibility of different components can be indicated by the Flory-Huggins interaction parameters (χ) [69], which can be afforded by the equation $\chi \propto (\sqrt{\gamma_{\text{A}}} - \sqrt{\gamma_{\text{D}}})^2$, where γ_{A} and γ_{D} represent surface tensions of donors and acceptors, respectively. The surface tension (γ) was determined to be 26.3, 26.8, 27.5, and 19.6 mN m^{-1} for TC-Th, BC-Th, BC-Th:L8-BO, and D18, respectively, by employing Wu's model [70,71]. As can be seen from Figure 6a and Table S8, the χ values of D:A blends are in order of TC-Th:D18 (0.49) < BC-Th:D18 (0.56) < BC-Th:L8-BO:D18 (0.67), indicating gradually decreased D/A miscibility and also coinciding with the increased domain sizes in TEM images from TC-Th:D18, BC-Th:D18 to BC-Th:L8-BO:D18. Moreover, the stability of two dimerized SMAs-based OSCs was also evaluated and compared. Note that the morphological stability is strongly determined by diffusion coefficients of SMAs [72,73] and the molecular diffusion properties can be indicated by proxy metrics such as glass transition temperatures (T_{g}) [74]. The T_{g} can be roughly estimated by measuring the UV-vis absorbance of molecules in films at various annealing temperatures (40–160 $^{\circ}\text{C}$) [75]. As shown in Figure 6b, c and Figure S11, BC-Th exhibits a much higher T_{g} of 102 $^{\circ}\text{C}$ than that of TC-Th (89 $^{\circ}\text{C}$), which should be main attributed to the slightly larger molar mass of BC-Th and the tighter inter-

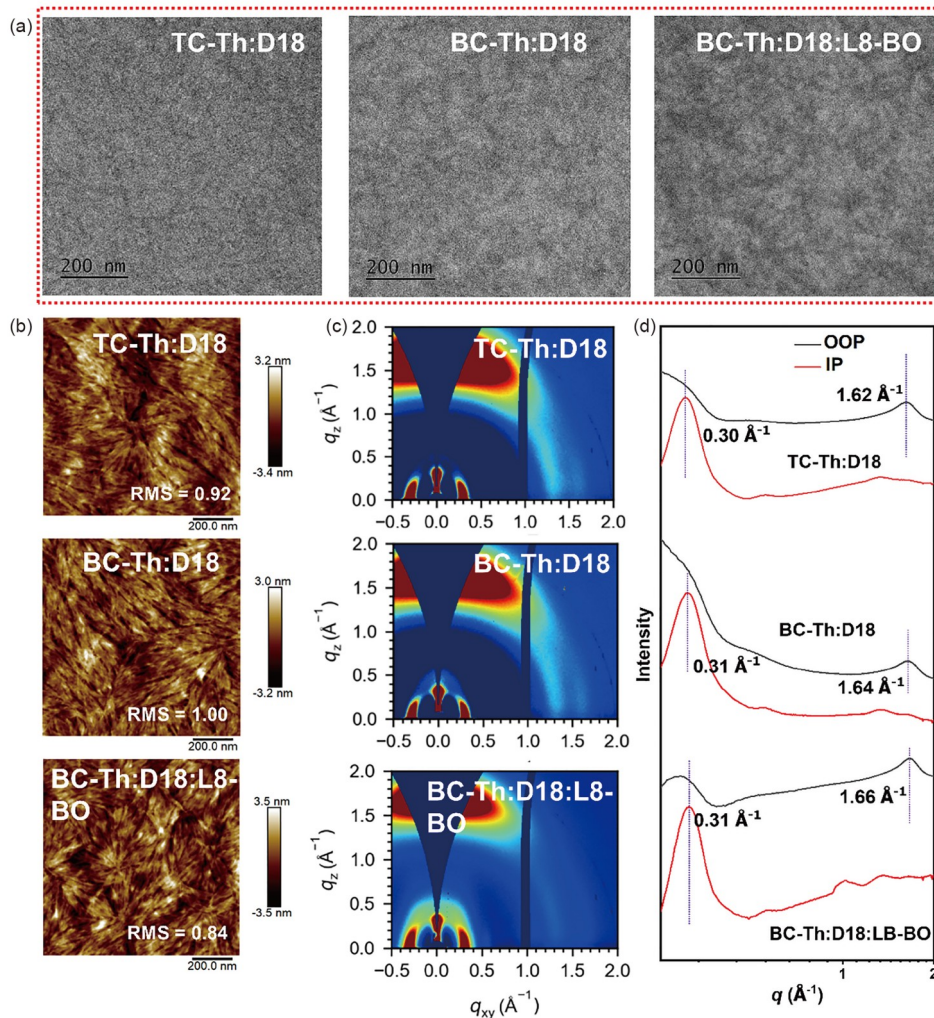


Figure 5 (a) TEM images and (b) AFM height images of all blended films. 2D GIWAXS images of (c) TC-Th:D18, BC-Th:D18, and BC-Th:D18:L8-BO blended films. (d) 1D GIWAXS profiles of TC-Th:D18, BC-Th:D18, and BC-Th:D18:L8-BO blended films (color online).

molecular packing in IP direction. In addition, the T_g (87 °C) of Y-Th is slightly lower than TC-Th due to its lower molecular weight. The higher T_g can inhibit molecular diffusion in D/A blends for de-mixing and maintaining better device stability [74]. Promisingly, the devices based on BC-Th and BC-Th:L8-BO afford a slightly better long-term stability than TC-Th-based ones (Figure S12). Furthermore, after being aged at 65 °C, it is evident that the BC-Th-based OSCs exhibit a larger T_{80} (more stable) of 372 h, followed by TC-Th-based OSCs with a T_{80} of 244 h (Figure 6d). In addition, the further improved stability of ternary OSCs after introducing a relative small acceptor molecule of L8-BO may be benefitting from the attenuated collapse of morphology in blended films that involving donor and acceptor components with quite large molecular sizes [76]. Moreover, it is evident that the stability of TC-Th and BC-Th is significantly better than that of Y-Th-based OSCs ($T_{80} = 192$), which is also our initial motivation for dimerizing small molecule acceptors.

3 Conclusions

To overcome the inferior device efficiencies of conventional terminal coupling dimerized (TC-type) SMAs-based OSCs, an exotic pathway (BC-type) to construct dimerized SMAs is explored by bridging the branched groups of two monomers (like BC-Th acceptor) rather than conventional terminals (like TC-Th counterpart). A comprehensive investigation has revealed that the BC-Th acceptor with BC-type architecture exhibits multiple molecular orientations along with a larger molar extinction coefficient, dielectric constant and electron mobility compared with that of TC-Th with TC-type architecture, which mainly benefits from the distinctive 3D conformation and less disturbed terminals in such a BC-type molecule. When blending with the D18 donor, more compact/ordered π - π stacking, obvious fibrillary network and efficient charge migration can be achieved in BC-Th blends compared with those of TC-Th. As a result, BC-Th:D18-based OSCs afford a superior PCE of 17.43%

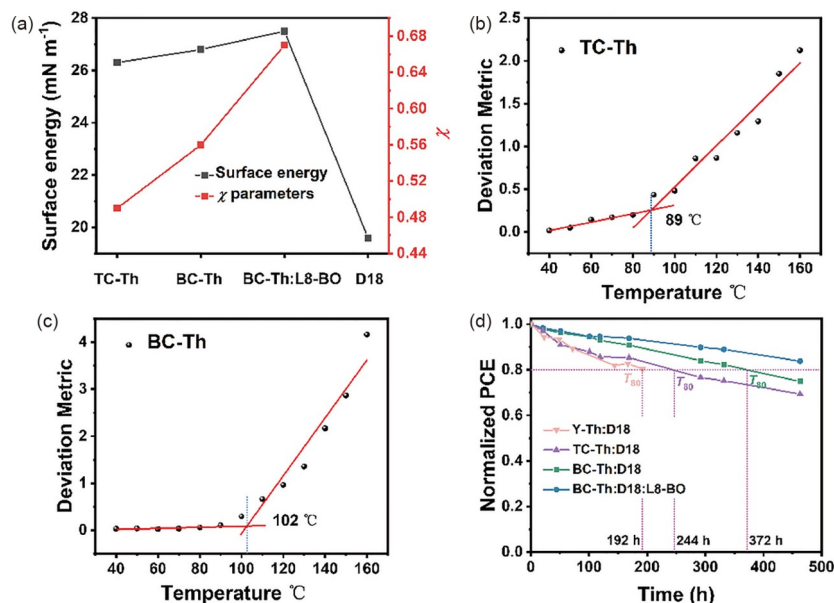


Figure 6 (a) Surface energy and calculated Flory-Huggins parameters by Wu's model. The glass transition temperature (T_g) of (b) TC-Th and (c) BC-Th. (d) Normalized PCEs of all OSCs after the TA at 65 °C for 450 h (color online).

and an excellent FF of 79.13% compared with the TC-Th:D18-based OSCs with a PCE of 16.29% and an FF of 74.81%. Notably, the FF based on BC-Th:D18 blends should be the highest value among dimerized SMAs-based OSCs reported to date, including both binary and ternary devices. Furthermore, the L8-BO, as the third component, was introduced to the BC-Th:D18 blends; overall enhanced performances are afforded with an efficiency of 18.05% and even higher FF of 80.11%. At last, BC-Th:D18-based devices exhibit better operational stability than TC-Th:D18-based ones. Furthermore, the BC-Th:D18:L8-BO-based ternary devices demonstrate further improved stability compared with the corresponding binary devices. By exploring such an exotic and efficient constructing strategy of dimerized SMAs, our work has provided a highly potential pathway to conquer the significant gap of FFs and even PCEs between dimerized SMAs-based OSCs and their monomer counterparts, thus boosting dimerized SMAs toward commercial applications further.

Acknowledgements This work was supported by the Ministry of Science and Technology of China (National Key R&D Program of China, 2022YFB4200400, 2019YFA0705900), the National Natural Science Foundation of China (21935007, 52025033, 22204119), Tianjin City (22JCQNJC00530) and Haihe Laboratory of Sustainable Chemical Transformations. The authors gratefully acknowledge the cooperation of the beamline scientists at the BSRF-1W1A beamline.

Conflict of interest The authors declare no conflict of interest.

Supporting information The supporting information is available online at chem.scichina.com and link.springer.com/journal/11426. The supporting materials are published as submitted, without typesetting or editing. The

responsibility for scientific accuracy and content remains entirely with the authors.

- Cai Y, Huo L, Sun Y. *Adv Mater*, 2017, 29: 1605437
- Inganäs O. *Adv Mater*, 2018, 30: 1800388
- Yao H, Hou J. *Angew Chem Int Ed*, 2022, 61: e202209021
- Jin J, Wang Q, Ma K, Shen W, Belfiore LA, Bao X, Tang J. *Adv Funct Mater*, 2023, 33: 2213324
- Lin Y, Wang J, Zhang ZG, Bai H, Li Y, Zhu D, Zhan X. *Adv Mater*, 2015, 27: 1170–1174
- Wang Y, Wang Y, Kan B, Ke X, Wan X, Li C, Chen Y. *Adv Energy Mater*, 2018, 8: 1802021
- Ke X, Meng L, Wan X, Li M, Sun Y, Guo Z, Wu S, Zhang H, Li C, Chen Y. *J Mater Chem A*, 2020, 8: 9726–9732
- Yuan J, Zhang Y, Zhou L, Zhang G, Yip HL, Lau TK, Lu X, Zhu C, Peng H, Johnson PA, Leclerc M, Cao Y, Ulanski J, Li Y, Zou Y. *Joule*, 2019, 3: 1140–1151
- Li C, Zhou J, Song J, Xu J, Zhang H, Zhang X, Guo J, Zhu L, Wei D, Han G, Min J, Zhang Y, Xie Z, Yi Y, Yan H, Gao F, Liu F, Sun Y. *Nat Energy*, 2021, 6: 605–613
- Liang H, Bi X, Chen H, He T, Lin Y, Zhang Y, Ma K, Feng W, Ma Z, Long G, Li C, Kan B, Zhang H, Rakitin OA, Wan X, Yao Z, Chen Y. *Nat Commun*, 2023, 14: 4707
- Zheng Z, Wang J, Bi P, Ren J, Wang Y, Yang Y, Liu X, Zhang S, Hou J. *Joule*, 2022, 6: 171–184
- Hu H, Ye L, Ghasemi M, Balar N, Rech JJ, Stuard SJ, You W, O'Connor BT, Ade H. *Adv Mater*, 2019, 31: 1808279
- Dong Y, Zou Y, Yuan J, Yang H, Wu Y, Cui C, Li Y. *Adv Mater*, 2019, 31: 1904601
- Baran D, Ashraf RS, Hanifi DA, Abdelsamie M, Gasparini N, Röhr JA, Holliday S, Wadsworth A, Lockett S, Neophytou M, Emmott CJM, Nelson J, Brabec CJ, Amassian A, Salleo A, Kirchartz T, Durrant JR, McCulloch I. *Nat Mater*, 2017, 16: 363–369
- Lee JW, Sun C, Lee C, Tan Z, Phan TNL, Jeon H, Jeong D, Kwon SK, Kim YH, Kim BJ. *ACS Energy Lett*, 2023, 8: 1344–1353
- Ghasemi M, Hu H, Peng Z, Rech JJ, Angunawela I, Carpenter JH, Stuard SJ, Wadsworth A, McCulloch I, You W, Ade H. *Joule*, 2019, 3: 1328–1348

- 17 Lee JW, Sun C, Kim DJ, Ha MY, Han D, Park JS, Wang C, Lee WB, Kwon SK, Kim TS, Kim YH, Kim BJ. *ACS Nano*, 2021, 15: 19970–19980
- 18 Sun C, Lee JW, Lee C, Lee D, Cho S, Kwon SK, Kim BJ, Kim YH. *Joule*, 2023, 7: 416–430
- 19 Li S, Zhang R, Zhang M, Yao J, Peng Z, Chen Q, Zhang C, Chang B, Bai Y, Fu H, Ouyang Y, Zhang C, Steele JA, Alshahrani T, Roeffaers MJB, Solano E, Meng L, Gao F, Li Y, Zhang ZG. *Adv Mater*, 2023, 35: 2206563
- 20 Meng X, Li M, Jin K, Zhang L, Sun J, Zhang W, Yi C, Yang J, Hao F, Wang G, Xiao Z, Ding L. *Angew Chem Int Ed*, 2022, 61: e202207762
- 21 Liu Y, Liu B, Ma CQ, Huang F, Feng G, Chen H, Hou J, Yan L, Wei Q, Luo Q, Bao Q, Ma W, Liu W, Li W, Wan X, Hu X, Han Y, Li Y, Zhou Y, Zou Y, Chen Y, Li Y, Chen Y, Tang Z, Hu Z, Zhang ZG, Bo Z. *Sci China Chem*, 2022, 65: 224–268
- 22 Lee JW, Sun C, Phan TNL, Lee DC, Tan Z, Jeon H, Cho S, Kwon SK, Kim YH, Kim BJ. *Energy Environ Sci*, 2023, 16: 3339–3349
- 23 Gu X, Zhang X, Huang H. *Angew Chem Int Ed*, 2023, 62: e202308496
- 24 Wang H, Cao C, Chen H, Lai H, Ke C, Zhu Y, Li H, He F. *Angew Chem Int Ed*, 2022, 61: e202201844
- 25 Sun G, Jiang X, Li X, Meng L, Zhang J, Qin S, Kong X, Li J, Xin J, Ma W, Li Y. *Nat Commun*, 2022, 13: 5267
- 26 Chen H, Zou Y, Liang H, He T, Xu X, Zhang Y, Ma Z, Wang J, Zhang M, Li Q, Li C, Long G, Wan X, Yao Z, Chen Y. *Sci China Chem*, 2022, 65: 1362–1373
- 27 Zhu W, Spencer AP, Mukherjee S, Alzola JM, Sangwan VK, Amsterdam SH, Swick SM, Jones LO, Heiber MC, Herzing AA, Li G, Stern CL, DeLongchamp DM, Kohlstedt KL, Hersam MC, Schatz GC, Wasielewski MR, Chen LX, Facchetti A, Marks TJ. *J Am Chem Soc*, 2020, 142: 14532–14547
- 28 Cao J, Yi L, Ding L. *J Semicond*, 2022, 43: 030202
- 29 Qi F, Li Y, Zhang R, Lin FR, Liu K, Fan Q, Jen AK. *Angew Chem Int Ed*, 2023, 62: e202303066
- 30 Sun C, Lee JW, Tan Z, Phan TNL, Han D, Lee HG, Lee S, Kwon SK, Kim BJ, Kim YH. *Adv Energy Mater*, 2023, 13: 2301283
- 31 Wang J, Cui Y, Xu Y, Xian K, Bi P, Chen Z, Zhou K, Ma L, Zhang T, Yang Y, Zu Y, Yao H, Hao X, Ye L, Hou J. *Adv Mater*, 2022, 34: 2205009
- 32 Yang T, Zhan C. *Sci China Chem*, 2023, 66: 2513–2531
- 33 Gu X, Wei Y, Yu N, Qiao J, Han Z, Lin Q, Han X, Gao J, Li C, Zhang J, Hao X, Wei Z, Tang Z, Cai Y, Zhang X, Huang H. *CCS Chem*, 2023, 5: 2576–2588
- 34 Zhang L, Zhang Z, Deng D, Zhou H, Zhang J, Wei Z. *Adv Sci*, 2022, 9: 2202513
- 35 Wang T, Chen M, Sun R, Min J. *Chem*, 2023, 9: 1702–1767
- 36 Liu F, Hou T, Xu X, Sun L, Zhou J, Zhao X, Zhang S. *Macromol Rapid Commun*, 2018, 39: 1700555
- 37 Luo Z, Liu T, Ma R, Xiao Y, Zhan L, Zhang G, Sun H, Ni F, Chai G, Wang J, Zhong C, Zou Y, Guo X, Lu X, Chen H, Yan H, Yang C. *Adv Mater*, 2020, 32: 2005942
- 38 He C, Chen Z, Wang T, Shen Z, Li Y, Zhou J, Yu J, Fang H, Li Y, Li S, Lu X, Ma W, Gao F, Xie Z, Coropceanu V, Zhu H, Bredas JL, Zuo L, Chen H. *Nat Commun*, 2022, 13: 2598
- 39 Zhang J, Tan CH, Zhang K, Jia T, Cui Y, Deng W, Liao X, Wu H, Xu Q, Huang F, Cao Y. *Adv Energy Mater*, 2021, 11: 2102559
- 40 Beljonne D, Pourtois G, Silva C, Hennebicq E, Herz LM, Friend RH, Scholes GD, Setayesh S, Müllen K, Brédas JL. *Proc Natl Acad Sci USA*, 2002, 99: 10982–10987
- 41 Ramirez I, Causa' M, Zhong Y, Banerji N, Riede M. *Adv Energy Mater*, 2018, 8: 1703551
- 42 Tang Z, Tress W, Inganäs O. *Mater Today*, 2014, 17: 389–396
- 43 Hou J, Inganäs O, Friend RH, Gao F. *Nat Mater*, 2018, 17: 119–128
- 44 Chen H, Zhang Z, Wang P, Zhang Y, Ma K, Lin Y, Duan T, He T, Ma Z, Long G, Li C, Kan B, Yao Z, Wan X, Chen Y. *Energy Environ Sci*, 2023, 16: 1773–1782
- 45 Rivnay J, Mannsfeld SCB, Miller CE, Salleo A, Toney MF. *Chem Rev*, 2012, 112: 5488–5519
- 46 Müller-Buschbaum P. *Adv Mater*, 2014, 26: 7692–7709
- 47 Liang H, Chen H, Wang P, Zhu Y, Zhang Y, Feng W, Ma K, Lin Y, Ma Z, Long G, Li C, Kan B, Yao Z, Zhang H, Wan X, Chen Y. *Adv Funct Mater*, 2023, 33: 2301573
- 48 Gao W, Fan B, Qi F, Lin F, Sun R, Xia X, Gao J, Zhong C, Lu X, Min J, Zhang F, Zhu Z, Luo J, Jen AK. *Adv Funct Mater*, 2021, 31: 2104369
- 49 Fu Z, Zhang X, Zhang H, Li Y, Zhou H, Zhang Y. *Chin J Chem*, 2021, 39: 381–390
- 50 Azimi H, Senes A, Scharber MC, Hingerl K, Brabec CJ. *Adv Energy Mater*, 2011, 1: 1162–1168
- 51 Marcus RA. *Angew Chem Int Ed Engl*, 1993, 32: 1111–1121
- 52 Guo Y, He L, Guo J, Guo Y, Zhang F, Wang L, Yang H, Xiao C, Liu Y, Chen Y, Yao Z, Sun L. *Angew Chem Int Ed*, 2022, 61: e202114341
- 53 Zhan L, Li S, Li Y, Sun R, Min J, Bi Z, Ma W, Chen Z, Zhou G, Zhu H, Shi M, Zuo L, Chen H. *Joule*, 2022, 6: 662–675
- 54 Kaiser C, Sandberg OJ, Zarrabi N, Li W, Meredith P, Armin A. *Nat Commun*, 2021, 12: 3988
- 55 Liu Q, Jiang Y, Jin K, Qin J, Xu J, Li W, Xiong J, Liu J, Xiao Z, Sun K, Yang S, Zhang X, Ding L. *Sci Bull*, 2020, 65: 272–275
- 56 Li S, Zhan L, Sun C, Zhu H, Zhou G, Yang W, Shi M, Li CZ, Hou J, Li Y, Chen H. *J Am Chem Soc*, 2019, 141: 3073–3082
- 57 Sun C, Qin S, Wang R, Chen S, Pan F, Qiu B, Shang Z, Meng L, Zhang C, Xiao M, Yang C, Li Y. *J Am Chem Soc*, 2020, 142: 1465–1474
- 58 Murgatroyd PN. *J Phys D-Appl Phys*, 1970, 3: 151–156
- 59 Gasparini N, Salvador M, Strohm S, Heumueller T, Levchuk I, Wadsworth A, Bannock JH, de Mello JC, Egelhaaf HJ, Baran D, McCulloch I, Brabec CJ. *Adv Energy Mater*, 2017, 7: 1700770
- 60 Cowan SR, Roy A, Heeger AJ. *Phys Rev B*, 2010, 82: 245207
- 61 Riedel I, Parisi J, Dyakonov V, Lutsen L, Vanderzande D, Hummelen JC. *Adv Funct Mater*, 2004, 14: 38–44
- 62 Kyaw AKK, Wang DH, Gupta V, Leong WL, Ke L, Bazan GC, Heeger AJ. *ACS Nano*, 2013, 7: 4569–4577
- 63 Sun Y, Nian L, Kan Y, Ren Y, Chen Z, Zhu L, Zhang M, Yin H, Xu H, Li J, Hao X, Liu F, Gao K, Li Y. *Joule*, 2022, 6: 2835–2848
- 64 Wang Y, Qian D, Cui Y, Zhang H, Hou J, Vandewal K, Kirchartz T, Gao F. *Adv Energy Mater*, 2018, 8: 1801352
- 65 Shockley W, Queisser HJ. *J Appl Phys*, 1961, 32: 510–519
- 66 Zhao H, Lin B, Xue J, Naveed HB, Zhao C, Zhou X, Zhou K, Wu H, Cai Y, Yun D, Tang Z, Ma W. *Adv Mater*, 2022, 34: 2105114
- 67 Hexemer A, Bras W, Glossinger J, Schaible E, Gann E, Kirian R, MacDowell A, Church M, Rude B, Padmore H. *J Phys-Conf Ser*, 2010, 247: 012007
- 68 Wang Z, Zhang Y, Zhang J, Wei Z, Ma W. *Adv Energy Mater*, 2016, 6: 1502456
- 69 Wang T, Brédas JL. *J Am Chem Soc*, 2021, 143: 1822–1835
- 70 Kim KH, Kang H, Kim HJ, Kim PS, Yoon SC, Kim BJ. *Chem Mater*, 2012, 24: 2373–2381
- 71 Comyn J. *Int J Adhes Adhes*, 1992, 12: 145–149
- 72 Ghasemi M, Balar N, Peng Z, Hu H, Qin Y, Kim T, Rech JJ, Bidwell M, Mask W, McCulloch I, You W, Amassian A, Risko C, O'Connor BT, Ade H. *Nat Mater*, 2021, 20: 525–532
- 73 Li N, Perea JD, Kassar T, Richter M, Heumueller T, Matt GJ, Hou Y, Güldal NS, Chen H, Chen S, Langner S, Berlinghof M, Unruh T, Brabec CJ. *Nat Commun*, 2017, 8: 14541
- 74 Qin Y, Balar N, Peng Z, Gadisa A, Angunawela I, Bagui A, Kashani S, Hou J, Ade H. *Joule*, 2021, 5: 2129–2147
- 75 Root SE, Alkhadra MA, Rodriguez D, Printz AD, Lipomi DJ. *Chem Mater*, 2017, 29: 2646–2654
- 76 Sun R, Wang W, Yu H, Chen Z, Xia XX, Shen H, Guo J, Shi M, Zheng Y, Wu Y, Yang W, Wang T, Wu Q, Yang YM, Lu X, Xia J, Brabec CJ, Yan H, Li Y, Min J. *Joule*, 2021, 5: 1548–1565